JOURNAL OF MATERIALS SCIENCE **38** (2003) 1307 – 1313

Study of the corrosion layer on iron obtained in solutions of water-polyethylene glycol (PEG 400)-sodium phosphate

Y. GOURBEYRE, E. GUILMINOT, F. DALARD*
Laboratoire d'Electrochimie et de Physico chimie des Materiaux et Interfaces (INPG/CNRS-UMR 5631), BP 75, Saint Martin d'Hères, France
E-mail: Francis.Dalard@lepmi.inpg.fr

The iron behaviour in phosphate/water/polyethylene glycol (PEG) was studied *in-situ* and *ex-situ* by spectrometry Raman, ESCA spectroscopy, X-ray diffraction, Auger spectroscopy were used as surface analysis methods. It changes with phosphate concentration. At low phosphate concentration (5×10^{-4} M-10^{-3} M-5×10^{-3} M), iron is corroded. The thin corrosion layer is a mixture of iron oxides (γ-Fe_2O_3, Fe_3O_4) and iron phosphate($Fe_3(PO_4)_2$, $8H_2O$). At high phosphate concentration (10^{-2} M-5×10^{-2} M), the iron is protected. The protection could be due to an heterogenous layer containing PEG 400 and phosphates.

1. Introduction

The different treatments used in iron and wood conservation and restoration are not always suitable for treating archaeological wood/iron composites. In fact, the alkaline solutions of sodium carbonate and sodium sulphite used in the chloride removal treatment of ferrous metals can attack the cellulose and cause damage to the wood parts. Solutions of poly(ethylene glycol) (PEG: HO-(CH_2-CH_2-O)$_n$-H) used to treat waterlogged wood are acidic (pH = 5.6) and lead to rapid corrosion of the metal [1]. The corrosion rate of iron in water+PEG 400 solutions depends on the PEG concentration [2]. Corrosion reaches a maximum in 20% (vol) PEG 400 solutions, which is in fact the concentration most commonly used by conservators for treating waterlogged artifact wood.

When treating composite artifacts, existing procedures have to be adapted, and since the wood is the most fragile of the materials, it would seem preferable to concentrate on treating the waterlogged wood while protecting the metal parts with an iron corrosion inhibitor.

A recent electrochemical study showed that phosphates already used as corrosion inhibiting agents in media containing glycol (cooling circuits), could be used to inhibit iron corrosion in water+PEG 400 solutions [3].

In aqueous solutions corrosion protection is provided by the passivating film composed of a mixture of iron oxides (Fe_3O_4, γ-Fe_2O_3 or FeOOH) with phosphates insertion [4, 5]. According to Pryor and Cohen [6], dissolved oxygen is adsorbed on the iron surface where it forms a thin film of iron oxide such as γ-Fe_2O_3. When the film is being formed, there is simultaneous electrochemical attack which can lead to the formation of compounds such as hydrated $FePO_4$ ($HPO_4^{2-} + Fe^{3+} \rightarrow FePO_4 + H^+$) in the presence of HPO_4^{2-} ions and Fe^{3+} ions. The corrosion process stops when the film is sufficiently uniform and thick to limit diffusion of the iron ions.

Other authors focus on HPO_4^{2-} ions, which are adsorbed on the metal surface. [5, 7, 8]. For these authors, the phosphate ions activate the iron oxidation and contribute to the growth of the passivating film according to the following equation:

- $3\,Fe + 2\,HPO_4^{2-} \rightarrow Fe_3(PO_4)_2 + 2\,H^+ + 6\,e^-$ (step 1)
- $Fe_3(PO_4)_2 + 4\,H_2O \rightarrow Fe_3O_4 + 2\,HPO_4^{2-} + 6\,H^+ + 2\,e^-$ (step 2)

A small quantity of phosphates in the oxide layers will increase the film density and enhance its protective properties [5]. However, if there are too many HPO_4^{2-} ions, they become incorporated in the oxides without forming iron phosphates. Then, they cause structural and electronic defects in the passive layer [9].

The cathodic reaction of dissolved oxygen reduction is not very sensitive to the phosphate concentration [3], unlike the anodic reaction. The phosphates thus behave as an anodic inhibitor reducing the anodic current and the number of anodic sites by oxide layer formation [10].

The structure of the oxide layer formed in presence of phosphates depends on the solution pH and on the anion concentration [11]:

$$H_2PO_4^-/HPO_4^{2-} \qquad pH = 7.19$$
$$HPO_4^{2-}/PO_4^{3-} \qquad pH = 12.09$$

*Author to whom all correspondence should be addressed.

Different techniques have been used to demonstrate the presence of two distinct layers within the passive film [5, 12, 13]. An inner layer—in contact with the metal-is composed of a mixture of iron oxides (such as Fe_3O_4, Fe_2O_3) and iron phosphates (such as vivianite $Fe_3(PO_4)_2 \cdot 8H_2O$ and/or $FePO_4 \cdot 2H_2O$). It blocks the surface of the metal reducing the anodic area and consequently the corrosion rate. The outer layer, which is in contact with the solution, is composed of corrosion products such as iron oxyhydroxides (FeOOH, $Fe(OH)_2$) and phosphate salts present in the solution incorporated in this layer This second more dense layer limits the diffusion of Fe^{2+}-Fe^{3+} ions, within a pH range of 7 to 9.

According to Sato *et al.* [11] and Szklarska-Smialowska and Staehle [12], there is no outer layer at acidic pH values (pH = 4.5). The inner layer is the only one formed, and this is not sufficient to protect the metal ($Fe_3PO_4 \cdot 8H_2O$ is porous). On the other hand, Melendres *et al.* [13] demonstrate the formation of an outer layer which they identify as iron phosphate $Fe(H_2PO_4)_2$ (the inner layer being the same as in the previous case).

For more alkaline pH values (pH = 12), there is only one layer, composed of Fe_3O_4 and PO_4^{3-} ions incorporated in the oxide layer [12, 13].

However, while numerous studies have investigated the mechanism of iron corrosion inhibition by phosphates in aqueous solutions, such a mechanism has not been determined in PEG+water solutions.

In this paper the iron behaviour obtained in PEG + water solution with increasing phosphate concentration was studied by analytic methods.

2. Experimental

2.1. Materials

Two types of iron specimens were used:

- A rod (Goodfellow, purity 98%) which was annealed for 40 hours at 1050°C, so as to obtain a microstructure similar to that of archaeological iron (iron with grain size of 50 μm). It was then fitted to a rotating electrode PTFE cap 2 mm in diameter.
- Plates (Goodfellow, purity 99.5%) $12.50 \times 12.50 \times 1.83$ mm in size.

Before each experiment, the specimens were polished with silicon carbide paper of increasingly finer grits (800, 2400, 4000) and then with 1 μm diamond-charged paste. They were then cleaned ultrasonically in alcohol.

2.2. Solutions

The solutions were prepared from a mixture of distilled water and 20% poly(ethylene glycol) 400. Some solutions also contained phosphates as the corrosion inhibitor in the form of $Na_2HPO_4 \cdot 12H_2O$ (Prolabo, pure for analyses) in concentrations ranging from 10^{-4} M to 5×10^{-2} M.

2.3. Electrochemical cell

The experiments were conducted in two types of cell:

- A double-walled three-electrode Metrohm cell placed in a Faraday cage thermostatically controlled at 25°C for the iron plates (working electrode). The counter electrode was a platinum grid.
- An electrochemical cell with a PTFE body specially designed for use with the Raman spectroscopy. The iron working electrode, inserted in the PTFE cap, was fitted to a micrometer set screw. It was possible to move it accurately during Raman analysis. A cover, carrying the counter electrode and a glass disk, was screwed to the body of the cell. The counter electrode was a platinum ring positioned above the working electrode allowing passage of the laser beam to observe the surface of the iron by Raman spectroscopy. The glass disk, 18.0 mm in diameter and between 130 and 180 μm thick protected the spectrometer lens from the solution. Two holes were made in the body of the cell. One was used for filling the cell, while the other was used to insert the reference electrode in an extension piece. The third hole in the cover was used to drain off any surplus solution. Sealing around the working electrode was provided by O-rings while epoxy resin was used to form a seal around the glass.

In both cases, the reference electrode was a saturated calomel electrode (SCE) ($E_{SCE} = 0.245$ V/SHE) which was connected to the cell by means of an extension piece filled with the test solution in order to limit pollution of the electrolyte.

2.4. Electrochemical measurements

The following apparatuses used to perform the electrochemical measurements:

- An EGG Instrument Model 273A potentiostat, controlled by Model 352 software,
- A Solartron 1287 potentiostat controlled by Corrware software (version 2.1–16).

The specimens were kept in the solutions for 5 hours at corrosion potential to allow the stabilisation and then the polarisation curves were measured from −50 mV below corrosion potential to +1.1 V/SCE at a scan rate of 1 mV/s.

The iron plates were oxidized in potentiostatic mode at +600 mV/SCE in water+PEG 400 solutions with different phosphate concentrations and with measured Faradic charge input in order to develop a reproducible corrosion layer.

2.5. Surface analysis methods

2.5.1. Raman spectroscopy

The specimens were polished and oxidized in a potentiostatic mode at +600 mV/SCE with measured Faradic charge input.

The *in-situ* Raman spectra were recorded on a Raman T64000 spectrometer (Jobin-Yvon) equipped with holographic networks with 1800 lines/mm resolving power, a microscope equipped with a ×50 long frontal lens (backscattering, microRaman), and a liquid nitrogen-cooled CCD detector. The laser intensity (HeNe; 632.8 nm) was 30 mW (approx. 3 mW at output on specimen). Integration time was 1 hour 20 minutes with 2 scans.

The *ex-situ* Raman spectra were recorded on a DILOR XY confocal spectrometer, using an Ar^+ ion laser, wave length 514.53 nm. The laser beam, arriving vertically on the specimen, was connected to a microscope with magnification set at ×100. The area analysed corresponded to a cylinder 0.7 μm in diameter and 1 μm thick.

2.5.2. ESCA

The samples were iron plates 12.5 × 11.0 × 1.83 mm in size, polished and oxidized as previously in potentiostatic mode at +600 mV/SCE with measured Faradic charge input.

The specimen was irradiated with soft monochromatic X photons (fluorescence line Mg Kα_{12} = 1.254 keV i.e, 0.989 nm). The analysed area corresponds to a cylindrical volume, diameter of approx. 6 mm and height of 10 atomic layers (1 to 5 nm). The analysis was performed in ultrahigh vacuum (pressure of $P < 10^{-7}$ Pa).

Energy calibration of the spectrometer (MAC 2 RIBER) was carried out on line 4f 7/2 of gold (83.8 eV) and the linearity of the scanning ramp was verified on lines Cu 2p 3/2 (932.8 eV) and Cu 3 s (122.9 eV).

We studied the evolution of the elemental composition of the specimen, from the surface through to the inside of the material, using ion sputter depth profiling (Ar^+ ion beam energy 3 keV). The sputter rate was in the range of 0.1 to 0.2 nm/min.

2.5.3. X-ray diffraction

The specimens were polished iron plates which had been immersed for 3 months at 50°C in solutions composed of water, 20% PEG 400 and Na_2HPO_4 phosphates in concentrations of 10^{-3} M, 5×10^{-3} M and 10^{-2} M.

The X-ray beam (Fe Kα = 6.404 keV, i.e. wavelength 0.1936 nm) was oriented with an angle of incidence of 5° so as to obtain pseudo-glancing observation conditions and limit penetration of X-radiation into the material. The information obtained would be for the surface layer about 1 to 5 μm thick.

2.5.4. Auger spectroscopy

The specimens (iron plates 12.50 × 11.00 × 1.83 mm in size) were polished and oxidized potentiostatically at +600 mV/SCE. The apparatus used was a PHI 670 SCANNING AUGER NANOPROBE (Perkin Elmer) spectrometer with a LaB6 field emission source. Ultra-vacuum conditions (10^{-8} Pa) were obtained by means of an ionic pump. The primary energy used was 1 to 20 keV with a beam current of 1 to 10 nA. Spatial resolution was 15 nm. A Cylindrical Mirror Analyser was used for analysis. Sputter depth profiles of the specimens were carried out at 2 keV with $\theta = 74°$ to improve resolution for the deeper areas. The profiles are given as a function of sputter time (0.2 nm/min).

3. Results and discussion

3.1. Accelerated iron corrosion tests in water + 20% PEG 400 + Na_2HPO_4 solutions. Influence of the phosphate ion concentration

Iron plate samples were corroded at 50°C for 3 months in water + 20% PEG 400 solutions containing Na_2HPO_4 at several concentrations (0, 10^{-3} M, 5×10^{-3} M, 10^{-2} M, 5×10^{-2} M, 10^{-1} M). After the test, the iron surface was only cleaned with distilled water and the (%) weight loss was determined.

We noticed (Table I) that the corrosion decreased when Na_2HPO_4 was added. The more concentrated the solution was, the lower the weight loss. With the addition of Na_2HPO_4 concentrations higher than 5×10^{-3} M, no weight loss variation was detected.

Iron ion concentration was then determined by ICP analysis (Table I). And in the same way iron ion concentrations decreased with the increase of Na_2HPO_4 concentration.

Addition of Na_2HPO_4 leads to an increase in the initial solution pH from pH = 5.5 (no addition) to pH = 8.6–8.8 (for concentration higher than 5×10^{-3} M).

Comparative pH measurements were made before and after corrosion tests (Table I). Without Na_2HPO_4 addition, the final pH value decreased, it reached pH = 4.4 which increased iron corrosion rate. With increasing Na_2HPO_4concentration, the final pH decreased was lower and no pH variation was obtained with 10^{-1} M Na_2HPO_4 concentration. At this final pH value (pH = 8.8), iron corrosion rate cannot increase.

In conclusion, when Na_2HPO_4 was added in the water + 20%PEG 400 solution, the corrosion rate of iron decreased. This result can be explained by phosphate ion properties or (and) pH increase.

We study the iron corrosion layer obtained in water + 20% PEG 400 solution with several Na_2HPO_4 additions in order to determine the major influence between phosphate additions and pH variations.

TABLE I Iron corrosion test in water + 20% PEG400 + Na_2HPO_4 solutions. Influence of the phosphate ion concentration on weight loss, iron ion in solution, pH values

C Na_2HPO_4 (M)	Δm (%)	(Fe^{2+}) (ppm)	Initial pH	Final pH
0	−24 ± 4	110 ± 10	5.5 ± 0.1	4.4 ± 0.1
10^{-3}	−14	40	7.5	4.5
5×10^{-3}	−0.2	3	8.0	7.0
10^{-2}	2.5	10	8.6	7.6
5×10^{-2}	0.2	1	8.6	8.0
10^{-1}	0.2	0.2	8.8	8.8

The corrosion solution used in this work can be separated into two categories: low concentration solutions ($\leq 5 \times 10^{-3}$ M) and high Na_2HPO_4 concentration solutions ($>5 \times 10^{-3}$ M).

3.2. At low phosphate ions concentrations (5×10^{-4} M, 10^{-3} M, 5×10^{-3} M)

A solution was prepared of water + 20% PEG 400 containing 5×10^{-4} M of Na_2HPO_4. An Auger electron spectroscopy analysis of an iron plate oxidized at +600 mV/SCE for 16 hours in this solution provides a concentration profile in atomic percent of the species present in the corrosion layer (Fig. 1). It reveals the presence of a carbon layer (98% at) coming from the PEG over a thickness of 0.4 nm.

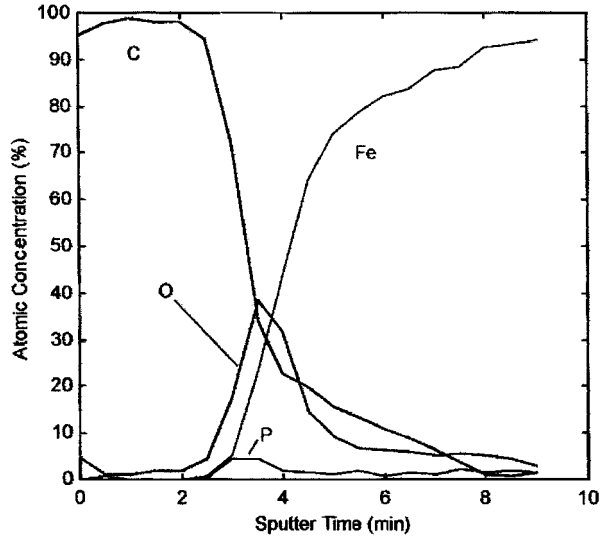

Figure 1 Auger electron spectroscopy concentration profile of corrosion layer on iron versus sputter time. Layer formation: +600 mV/SCE in H_2O + PEG 400 (20% v) + Na_2HPO_4 5×10^{-4} M for $t = 16$ h.

Deeper into the specimen, a significant increase in oxygen content occurred (40% at). We noticed the presence of phosphorus (5% at) and iron (15% at) over a thickness of 0.6 nm (after 0.8 nm sputtering). Finally, the carbon, oxygen and phosphorus contents drop while the iron content increases, reaching 95% at of metallic iron after 1.8 nm.

The iron specimens were immersed for 3 months in solutions of water+PEG 400 and Na_2HPO_4 with phosphate concentrations of 0 M, 10^{-3} M, 5×10^{-3} M. They were stored for 1 month (in a dry place) in a box containing a drying gel, then, examined by X-ray diffraction. Fig. 2 shows the evolution of the diffraction patterns as a function of the different phosphate concentrations.

Two main lines at 57° and 85° can be seen on all the spectra, corresponding to the metallic iron of a substrate. The second line for iron at 85° seems less intense for phosphate concentration of 5×10^{-3} M than for 10^{-3} M. This may be because the layer was thicker but it may also be due to its heterogeneity.

Without any Na_2HPO_4 (a), the lines correspond to different iron oxides: goethite (α-FeOOH) at 27° and 46°, hematite (α-Fe_2O_3) at 30°, 42°, 52°, 63°, 70°, 83°, and magnetite (Fe_3O_4) at 38°, 45°, 55°, 73°, 81°.

At a concentration of 10^{-3} M of Na_2HPO_4 (b), we notice that the spectrum is essentially composed of lines corresponding to the iron oxides: magnetite Fe_3O_4 (38°, 45°, 55°, 73°, 81°) and maghemite γ-Fe_2O_3 (38°, 45°, 55°, 74°, 82°) and those of metallic iron (57° and 85°). A few lines might correspond to phosphate species such as Na_3PO_4 (43°, 63°) although it was not initially present in the solution. A peak near the main peak for iron at 55° could correspond to an iron phosphate

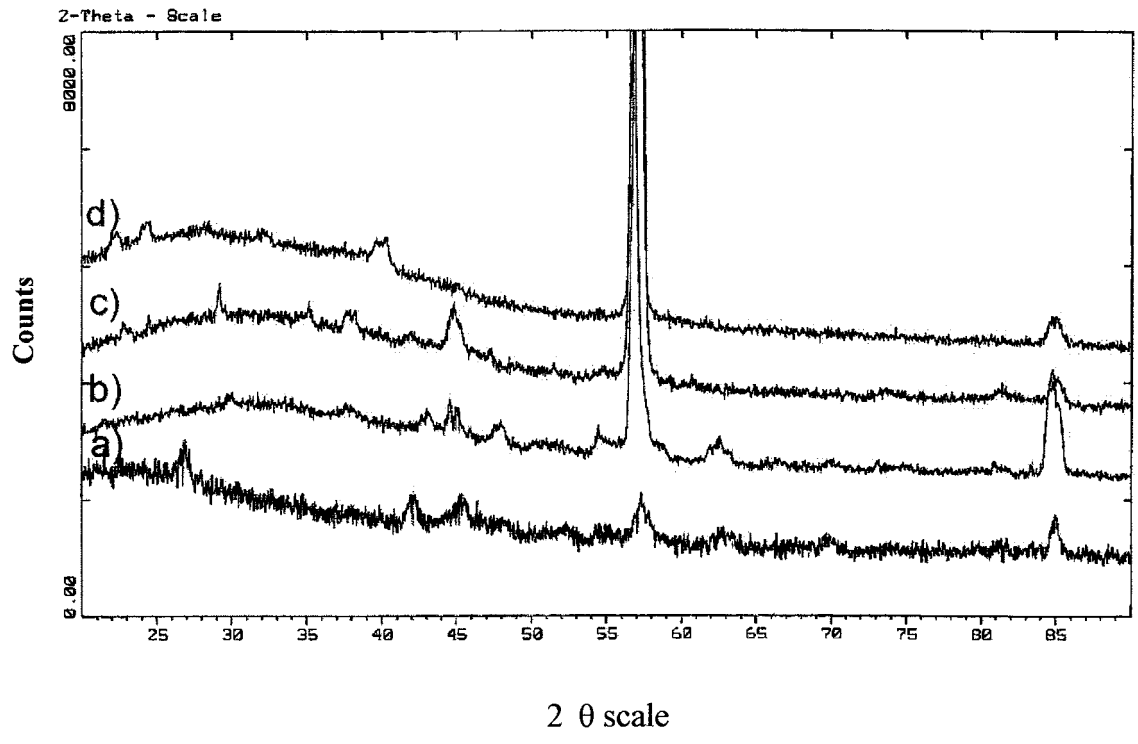

Figure 2 Influence of Na_2HPO_4 concentration on diffraction pattern for iron corrosion layer. Corrosion layer formation: iron plate during 3 months in H_2O + PEG 400 (20% v) + Na_2HPO_4 (Temperature: 298 K): (a) 0 M; (b) 10^{-3} M; (c) 5×10^{-3} M; (d) 10^{-2} M.

($Fe_4(PO_4)_3(OH)_3$), but it is not possible to conclude without further peaks for this compound.

At a higher concentration (5×10^{-3} M), the spectrum (c) still shows the peaks for iron (metallic) and magnetite. The other peaks can be identified as belonging to vivianite $Fe_3(PO_4)_2{,}8H_2O$ (18°, 24, 5°, 29°, 35°, 38°, 42°, 45°, 47°) which would correspond to the results in the literature [14]. The peak near the main peak for iron-present in the previous spectrum-can again be seen on this spectrum but here it is more pronounced.

According to the analyses performed, it appears that for low Na_2HPO_4 concentrations (5×10^{-4} M to 5×10^{-3} M), iron was covered with a mixture of iron phosphates and iron oxides. This result is in agreement with similar analyses in aqueous solutions reported in the literature. The presence of phosphate was unquestionable but the identification of the compounds was not clear. The formation of corrosion products seems to be influenced by PEG at low concentrations of Na_2HPO_4.

3.3. At high concentrations of phosphate ions (10^{-2} M and 5×10^{-2} M)

At the highest concentration (10^{-2} M) (Fig. 2d), the main iron peaks on the X-ray diffraction pattern are still present, but the peaks for iron oxides completely disappear. The remaining peaks may correspond to various phosphate species: $Na_3HP_2O_6{,}9H_2O$ (24°, 40°), $FePO_4$ (32°), $Na_2HPO_4{,}7H_2O$ (40°) present initially in the solution. The peak near of the main iron peak is still more pronounced than for the previous spectra, suggesting sensitivity to the phosphate concentration.

An iron plate was oxidized at +600 mV/SCE for 16 hours in a solution of water+PEG 400 (20% volume) with 5×10^{-2} M Na_2HPO_4 then rinsed in alcohol. The Faradic charge measured during the treatment was 66 C/m^2. The thickness of the layer was estimated assuming that it was formed of only one compound and that the layer was uniform. Our estimates were based on the compounds $FePO_4{,}2H_2O$, Fe_2O_3, Fe_3O_4. The specimen was observed using SEM. Fig. 3 shows a heterogeneous layer with two areas:

- A fairly small dark area in which X-ray microanalysis reveals the presence of high concentrations of carbon, iron, oxygen, phosphorus and sodium.
- A light area containing the same elements, but less carbon compared to the dark area.

Observations using an atomic force microscope (AFM) allowed us to estimate the thickness of the dark layer which appeared to be about 200 nm.

The same specimen was analysed *ex-situ* by Raman spectroscopy. The light area gave no interpretable signal, possibly because the layer was too thin. The dark area provided some additional information (Fig. 4b).

The main line at 936 cm^{-1} (spectrum 4b) can be characteristic of phosphates. This line corresponds to the line at 980 cm^{-1} in the spectrum (4a), obtained for solid Na_2HPO_4 and depends on the crystalline environment. The shift of 40 cm^{-1} is induced by the following crystalline changes: ions HPO_4^{2-} in solid Na_2HPO_4 become PO_4^{3-} in spectrum (4b). The other lines-spectrum (4b)-attributed to phosphate are near to 861 cm^{-1} and 560–590 cm^{-1} [14]. The lines at 1060, 1130, 1290, 1410 cm^{-1} correspond respectively to C─C bonds and C─H bond of PEG. The lines at 230 and 500 cm^{-1} can be attributed to Fe_2O_3 [15] and the line at 400 cm^{-1} to FeOOH. Fe_3O_4 is identified at 687 and 711 cm^{-1}.

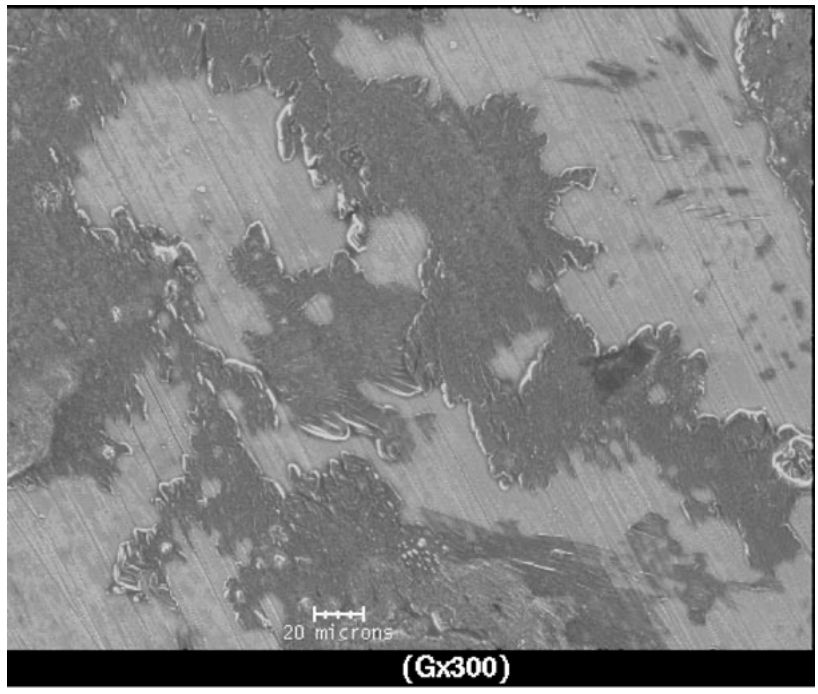

Figure 3 SEM photography of iron corrosion layer (×300). Layer formation: +600 mV/SCE in H_2O + PEG 400 (20%) + Na_2HPO_4 5×10^{-2} M for $t = 16$ h.

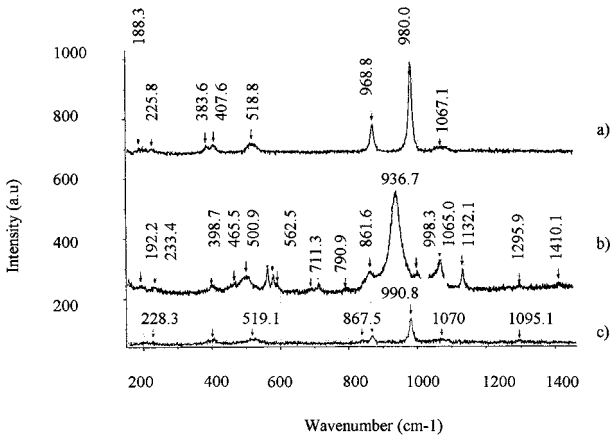

Figure 4 Ex-situ Raman spectrum a—Na_2HPO_4, b—iron corrosion layer rinsed out by ethyl alcohol. Layer formation: +600 mV/SCE in H_2O + PEG 400 (20%) + Na_2HPO_4 5×10^{-2} M for $t = 16$ h.

The results of *ex-situ* Raman analysis suggested—for dark area—the existence of a complex mixture of iron oxides (Fe_2O_3 and FeOOH), phosphates and PEG.

An ESCA analysis was conducted on an iron plate oxidized at +600 mV/SCE in a mixture of water + PEG 400 (20%) with a Na_2HPO_4 concentration of 5×10^{-2} M. The faradic charge input (19 C/m^2) was controlled in order to lead to a 5 nm layer considering a 236 mm^2 specimen surface and $FePO_4$ as the only product formed. The specimen was rinsed in absolute alcohol prior to the observation.

The first spectrum (Fig. 5) which was obtained before ion sputtering, shows the phosphorus photopeaks (P_{2p} and P_{2s}) and the Auger transitions of sodium. Oxygen photopeak 1s is very pronounced, as are its Auger transitions. On the contrary, the photopeaks of iron (Fe_{2p}) and the Auger transitions are very attenuated. Photopeak C_{1s} of carbon can also be observed. Furthermore, the energy position of the photopeaks Fe_{2p} of iron (710 eV and 725 eV) indicates a signal for ferric oxide (Fe_2O_3).

After sputtering to 2 to 3 nm, the presence of phosphorus and sodium can still be observed, whereas carbon has disappeared. The iron photopeaks and the Auger transitions were more intense.

The crystalline iron oxide represents the main form of iron, but pure iron Fe° photopeak can also be observed.

After 20 minutes of ion sputtering (3 to 4 nm), the spectrum contained no traces of carbon. The phosphates were in low concentration (residues of O_2 and $Na_{(A)}$). The signal for metallic iron was predominant, though the iron oxide was still present. After 6 nm sputtering, the spectrum corresponds to metallic iron with traces of oxygen. This spectrum suggested that the specimen was pure iron (no foreign elements or trace elements).

ESCA analysis of a specimen freshly polished to a tenth of a micron and rinsed in absolute alcohol gave photopeaks and Auger transitions for iron, oxygen, carbon and sodium. Iron is mostly bound in the ferric oxide Fe_2O_3, though there is also a signal corresponding to metallic iron suggesting that the oxide layer is thin.

After 20 minute sputtering, the spectrum corresponds to a specimen of pure iron. The oxide layer thickness is between 3 and 4 nm.

To complete our study, electrochemical analysis and Raman spectroscopy were used to perform *in-situ* measurements. The Raman cell was first validated electrochemically for solutions with 10^{-3} M Na_2HPO_4.

An iron electrode was polarised at +600 mV/SCE for 10 hours in the Raman cell in the presence of water+PEG 20% (vol) and Na_2HPO_4 (5×10^{-2}M).

After this treatment, the specimen was observed under an optical microscope and analysed *in-situ* by Raman spectroscopy. "Gelatinous" deposits were observed on the specimen. When the laser beam was focused on these deposits, spectrum (b) shown in Fig. 6 was obtained. Spectrum (a) shows the characteristic signature of PEG presenting peaks at 527 cm^{-1}, 806-840-887 cm^{-1} (C—O—C bond), 1040-1061-1130 cm^{-1} (C—C bond), 1238 cm^{-1}, 1283 cm^{-1}, 1473 cm^{-1} (CH_2 or O—CH_2 bond), 1650 cm^{-1}.

Comparison of spectrum (6a) and spectrum (6b) reveals that the peaks on spectrum (6b) are in the most

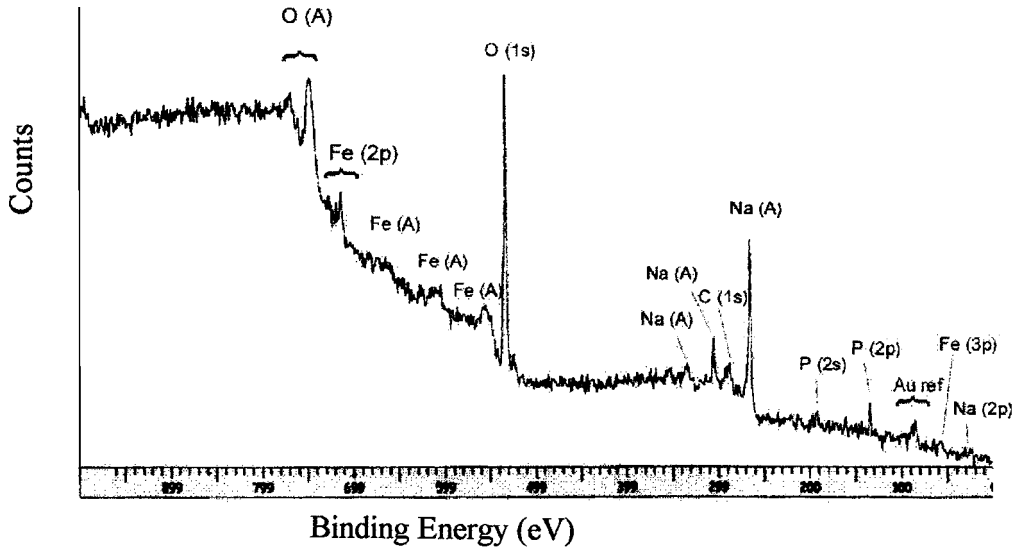

Figure 5 ESCA analysis of iron corrosion layer before ionic sputtering. Layer formation: +600 mV/SCE, Q = 13 C · m^{-2} in H_2O + PEG 400 (20%) + Na_2HPO_4 5×10^{-2} M.

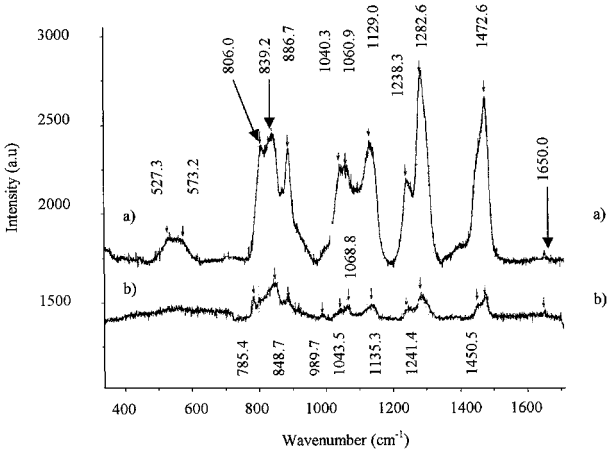

Figure 6 In-situ Raman spectrum. a) Pure PEG 400. b) Iron corrosion layer. Layer formation: +600 mV/SCE in H_2O + PEG 400 (20%) + Na_2HPO_4 5×10^{-2} M for $t = 10$ h.

part those of PEG. However, there is also a slight displacement of certain peaks for PEG ($\sim$5 cm^{-1}) along with a change in shape and intensity.

Only two peaks do not correspond to these of PEG: 785 cm^{-1}, belonging to a phase not yet identified, and 990 cm^{-1} which could correspond to phosphates [13].

However, there is also a slight displacement of certain peaks for C–O–C bonds ($\sim$5 cm^{-1}) along with a change in shape and intensity resulting from a possible change in the PEG environment (complexation, gelification).

These results with *in-situ* Raman are obtained on the apparatus with lower resolution than the *ex-situ* Raman measurements (Fig. 4b). The lack of iron oxides and phosphate ions peaks for the *in-situ* analysis can be explained by the fact that we did not analyse the surface layer but the solution.

The results at high phosphate concentrations are different from those obtained in a dilute aqueous solution. The presence of iron is insignificant and difficult to detect by XRD analysis or by ESCA. The thickness of iron oxide layer is nearly the same than that on polished or oxidized surface at +600 mV/SCE in a solution PEG 20% and 5×10^{-2} M Na_2HPO_4. PEG changed the formation of the corrosion layer.

The SEM analysis proves the heterogenous composition of the layer, with a content of carbon. The other analyses (ESCA and Raman) also indicate the presence of PEG in this layer. The PEG structure change near the surface (*in-situ* Raman analysis) could be induced by phosphate ions. In fact, in water-PEG solutions, the interactions between water and the PEG through hydrogen bonding enable water to surround the PEG chains. But the addition of salts can modify the hydrated structure of the polymer by causing segregation. The influence of an anion on PEG depends on its affinity with water, characterised by its lyotropic number. An anion with a low lyotropic number such as PO_4^{3-} ($n = 3.2$), can form a second phase with PEG [14]. Some cations [15]—such as Na^+-increase the anisotropy of its configuration by creating strong bonds with PEG and forming complexes (crown ether type) [16]. Segregation is even more marked when the salt concentration is high.

This segregation induced the formation of a new phase with PEG and PO_4^{3-}, this layer plays a major effect during iron corrosion in water-PEG solutions.

4. Conclusions

In our study, we used different techniques (*ex-situ* and *in-situ* Raman spectroscopy, ESCA, Auger spectroscopy, X-ray diffraction, SEM, X-ray microanalysis) to analyse the corrosion layer formed on iron in water+ PEG 400 solutions in the presence of phosphates (Na_2HPO_4).

We noticed that at low phosphate concentrations (from 5×10^{-4} M to 5×10^{-3} M), the corrosion layer is composed of a mixture of iron oxides (γ-Fe_2O_3, Fe_3O_4) and iron phosphates (vivianite $Fe_3(PO_4)_2$, $8H_2O$). These results are in agreement with literature data for iron corrosion in aqueous phosphate solutions.

At higher phosphate concentration (10^{-2} M to 5×10^{-2} M), the iron oxides almost totally disappear. Only a thin iron oxide layer, formed when iron is exposed to air, was present. Corrosion was inhibited by the layer composed of PEG and phosphates resulting from segregation of the PEG, the phosphates being at sufficient concentrations to promote this phenomenon.

References

1. L. S. SELWYN, D. A. RENNIE-BISAILLION and N. E. BINNIE, *Studies in Conservation* **38** (1993) 180.
2. E. GUILMINOT, F. DALARD and C. DEGRIGNY, Materials Corrosion and Protection, session ISE/EFC Conference, Proceeding 50th ISE Meeting, Pavia, Italy, 5–10 September, 1999.
3. E. GUILMINOT, F. DALARD and C. DEGRIGNY, Proceedings of the 9th SEIC, Ferrara, Italy, 4–8th September 2000.
4. J. E. O. MAYNE and J. W. MENTER, *J. Chem. Soc.* (1954) 103.
5. W. KOZLOWSKI and J. FLIS, *Corros. Sci.* **32** (1991) 861.
6. M. J. PRYOR and M. COHEN, *J. Electrochem. Soc.* **98** (1951) 263.
7. K. OGURA and T. MAJIMA, *Electrochim. Acta* **23** (1978) 1361.
8. J. G. N. THOMAS, *British Corros. J.* **1** (1966) 156.
9. K. AZUMI, T. OHTSUKA and N. SATO, *J. Electrochem. Soc.* **134** (1987) 1352.
10. M. J. FRANKLIN, D. C. WHITE and H. S. ISAACS, *Corros. Sci.* **33** (1992) 251.
11. N. SATO, K. KUDO and T. NODA, *Zeiteschrift für Physikalische Chemie Neue Folge* (*Z. Phys. Chem.*) **98** (1975) 271.
12. Z. SZKLARSKA-SMIALOWSKA and R. W. STAEHLE, *J. Electrochem. Soc.* **121** (1974) 1393.
13. C. A. MELENDRES, N. CAMILLONE III and T. TIPTON, *Electrochim. Acta* **34** (1989) 281.
14. D. L. A. DE FARIA, S. VENÂNCIO SILVA and M. T. DE OLIVEIRA, *J. Raman Spectro.* **28** (1997) 873.
15. A. HUGOT-LE GOFF, J. FLIS, N. BOUCHERIT, S. JOIRET and J. WILINSKI, *J. Electrochem. Soc.* **137** (1990) 2684.
16. F. E. BAILEY, J. KOLESKE, Alkylene oxides and their polymers, 35 Ed. Marcel Dekker, New-York, 1991).

Received 8 January
and accepted 10 October 2002